

Theory of Spin Exciton in the Kondo Semiconductor YbB_{12}

Alireza Akbari,^{1,4} Peter Thalmeier,² and Peter Fulde^{1,3}

¹Max Planck Institute for the Physics of Complex Systems, D-01187 Dresden, Germany

²Max Planck Institute for Chemical Physics of Solids, D-01187 Dresden, Germany

³Asia Pacific Center for Theoretical Physics, Pohang, Korea

⁴Institute for Advanced Studies in Basic Sciences, 45195-1159 Zanjan, Iran

(Received 22 October 2008; published 10 March 2009)

The Kondo semiconductor YbB_{12} exhibits a spin and charge gap of approximately 15 meV. Close to the gap energy narrow dispersive collective excitations were identified by previous inelastic neutron scattering experiments. We present a theoretical analysis of these excitations. Starting from a periodic Anderson model for crystalline-electric-field- (CEF) split $4f$ states we derive the hybridized quasiparticle bands in slave boson mean-field approximation and calculate the momentum dependent dynamical susceptibility in random phase approximation. We show that a small difference in the hybridization of the two CEF (quasi-) quartets leads to the appearance of two dispersive spin resonance excitations at the continuum threshold. Our theoretical analysis explains the most salient features of previously unexplained experiments on the magnetic excitations of YbB_{12} .

DOI: 10.1103/PhysRevLett.102.106402

PACS numbers: 71.27.+a, 75.40.Gb, 71.70.Ch

The so-called Kondo insulators or semiconductors like, e.g., CeNiSn , SmB_6 and YbB_{12} represent a special class of strongly correlated electrons [1]. In these compounds the conduction electrons hybridize with nearly localized $4f$ electrons. The Coulomb repulsion of the latter results in a small energy gap [2] of order 10 meV at the Fermi level [3,4]. At temperatures higher than the gap energy these materials behave like Kondo metals exhibiting their typical spin fluctuation spectrum. But at low temperatures a spin and charge gap opens indicating the formation of an insulating singlet ground state [1,5]. This may be concluded from the total suppression of the local moment in the susceptibility and from the semiconducting behavior of the resistivity, respectively [6]. The gap formation may also be seen directly in the dynamical susceptibility and finite frequency conductivity as probed in inelastic neutron scattering (INS) and optical conductivity experiments. In cubic YbB_{12} the spin [7] and charge [8] gap obtained in this way are approximately equal to 15 meV but in general they need not be identical.

In addition unpolarized [9] and polarized [7] INS has found an interesting dispersive fine structure around this threshold energy. Three excitation branches have been identified with energies 15, 20, and 38 meV, respectively, by analyzing the spectral function of the dynamical susceptibility. Since the lower two INS peaks are narrow and mostly centered at the zone boundary L point with $\mathbf{Q} = (\pi, \pi, \pi)$ they may be associated with the formation of a collective heavy quasiparticle spin resonance exciton appearing around the spin gap threshold [7,9] and driven by heavy quasiparticle interactions. The collective modes remain visible in the 20 meV region up to $T = 159$ K [10,11]. Similar spin resonance phenomena appear as result of feedback effect in unconventional heavy-fermion superconductors below the quasiparticle continuum thresh-

old at $2\Delta_0$ where Δ_0 is the gap amplitude [12]. The upper peak is much broader and shows little dispersion. It is also rapidly suppressed with increasing temperature. It has been associated with continuum excitations [13] also visible in a broad maximum in the optical conductivity [8] around 38 meV.

These intriguing experimental results have commonly been interpreted in a qualitative way within the spin exciton scenario [7,9,15] but an alternative model was also proposed [16]. However no analysis of the former was attempted so far although it is of fundamental importance to understand the microscopic origin and fine structure of the spin gap in Kondo semiconductors. In this communication we show in detail how the spin exciton bands in YbB_{12} arise on the background of a single-particle continuum at the spin gap edge. We discuss the origin of the splitting into two modes, its connection to crystalline-electric-field- (CEF) effects as well as their spectral shape and dispersion. Our investigations clarify the underlying microscopic physics of these intriguing and for a long time unexplained observations.

Our starting point is the hybridization-gap picture based on the periodic Anderson model which is the most widely accepted for the description of Kondo semiconductors. Using the mean-field slave boson approximation for CEF split $4f$ states of Yb we calculate the hybridized bands. With an empirical model for the quasiparticle interactions we evaluate the momentum dependent dynamical magnetic susceptibility in random phase approximation (RPA). Its imaginary part is proportional to the INS spectrum. We obtain sharp resonance features around the continuum threshold and wave vectors not too far from the zone boundary L point. Away from this point the resonance peaks disperse upwards in energy and broaden. They merge into the single particle continuum less than halfway

into the Brillouin zone (BZ), which describes the basic experimental facts. In addition our calculation suggests that CEF splitting and associated CEF orbital dependence of hybridization are responsible for the observed splitting into two dispersive resonance modes.

The Yb electronic configuration is $4f^{13}$ corresponding to a single hole in the $4f$ -shell [14]. Therefore we consider the Anderson lattice model with a f -hole in a $j = 7/2$ state, including the CEF effect, i.e., $H_t = H_f + H_d + H_{f-d} + H_C$. Here H_f describes the lattice of the localized, CEF-split $4f$ holes, H_d the conduction electrons and H_{f-d} is the hybridization between both. Finally H_C is the Coulomb interaction with an on-site hole repulsion U_{ff} . Our model assumes the limit $U_{ff} \rightarrow \infty$ where doubly occupied (hole) states ($4f^{12}$) are excluded and the two possible Yb configurations are either $4f^{14}$ or $4f^{13}$. The one without a $4f$ hole, i.e., $4f^{14}$ can be accounted for by an auxiliary boson b_i^\dagger [17]. In cubic symmetry the $j = 7/2$ multiplet is split by the CEF into a quartet Γ_8 ground state and two excited doublet states. The latter may be treated as a quasi quartet Γ'_8 according to INS results at higher temperatures [18]. The two quartets (index $\Gamma = 1, 2$) have energies $\Delta_1 = 0$ and $\Delta_2 > 0$. The model Hamiltonian in the restricted zero- and one- hole Hilbert space is then

$$H = \sum_{i\gamma} (\epsilon_f + \Delta_\gamma) f_{i\gamma}^\dagger f_{i\gamma} + \sum_{\mathbf{k}\gamma} \epsilon_{\mathbf{k}} d_{\mathbf{k}\gamma}^\dagger d_{\mathbf{k}\gamma} + N_s^{-1/2} \sum_{i\mathbf{k}\gamma} (V_{\mathbf{k}\gamma} e^{i\mathbf{k}\cdot\mathbf{R}_i} f_{i\gamma}^\dagger d_{\mathbf{k}\gamma} b_i + \text{c.c.}), \quad (1)$$

Here $\gamma = (\Gamma, m)$ where $\Gamma = 1, 2$ denotes the quartets and $m = 1-4$ is the orbital degeneracy index. Furthermore the local constraint $\tilde{Q}_i = b_i^\dagger b_i + \sum_\gamma f_{i\gamma}^\dagger f_{i\gamma} = 1$ has to be respected for all i . Therefore the total Hamiltonian including the constraint is $H - \lambda_b \sum_i (\tilde{Q}_i - 1)$, where λ_b is the Lagrange multiplier. Here the $f_{i\gamma}^\dagger$ create f -holes at lattice sites i in CEF state γ , and the $d_{\mathbf{k}\gamma}^\dagger$ create the holes in the conduction band with wave vector \mathbf{k} and CEF state index γ . The f -orbital energy is ϵ_f , while $\Delta_\gamma = \Delta_\Gamma$ is the CEF excitation energy, and N_s is the number of lattice sites. Finally $V_{\mathbf{k}\gamma}$ is the hybridization energy between $4f$ and conduction holes. In the following, the \mathbf{k} dependence of the hybridization energy is neglected, i.e., $V_{\mathbf{k}\gamma} = V_\gamma$. This is justified for a fully gapped Kondo insulator like YbB₁₂ where $V_{\mathbf{k}\gamma}$ does not vanish along lines in \mathbf{k} space. Furthermore to use only a minimum set of model parameters, we replace $V_\gamma = V_{\Gamma,m}$ by $V_\Gamma = \frac{1}{2}(\sum_m |V_{\Gamma,m}|^2)^{1/2}$ which is the average over each set of quartet states. We use a nearest-neighbor tight binding model with hopping t for the conduction electron bands $\epsilon_{\mathbf{k}}$. The spectral function of the experimental dynamical susceptibility of YbB₁₂ exhibits two sharp peaks [7]. Therefore it is essential that the two CEF quartets have two different average hybridization energies V_Γ ($\Gamma = 1, 2$).

The mean-field approximation to Eq. (1) is obtained by taking $b = \langle b_i \rangle$. Minimizing the ground state energy with respect to b and the Lagrange multiplier λ_b leads to the equations

$$\lambda_b b = \sum_\gamma V_\gamma W_\gamma; \quad \sum_\gamma n_\gamma^f + b^2 = 1; \quad n = \sum_\gamma (n_\gamma^d + n_\gamma^f), \quad (2)$$

where the following expectation values are introduced $W_\gamma = \frac{1}{N_s} \sum_{\mathbf{k}} \langle f_{\mathbf{k}\gamma}^\dagger d_{\mathbf{k}\gamma} \rangle$, $n_\gamma^d = \frac{1}{N_s} \sum_{\mathbf{k}} \langle d_{\mathbf{k}\gamma}^\dagger d_{\mathbf{k}\gamma} \rangle$ and $n_\gamma^f = \frac{1}{N_s} \sum_{\mathbf{k}} \langle f_{\mathbf{k}\gamma}^\dagger f_{\mathbf{k}\gamma} \rangle$. In Eq. (2), n is the density of holes per site which defines the chemical potential μ . The mean-field Hamiltonian can be diagonalized. One obtains, $H_{\text{MF}} = \sum_{\mathbf{k}\gamma,\pm} E_{\gamma,\pm}(\mathbf{k}) a_{\mathbf{k}\gamma,\pm}^\dagger a_{\mathbf{k}\gamma,\pm}$, where the hybridized bands have energies $E_{\gamma,\pm}(\mathbf{k}) = \frac{1}{2}[\epsilon_{\mathbf{k}} + \bar{\epsilon}_{f_\gamma} \pm \sqrt{(\epsilon_{\mathbf{k}} - \bar{\epsilon}_{f_\gamma})^2 + 4\bar{V}_\gamma^2}]$ which are still fourfold ($m = 1-4$) degenerate. The corresponding $4f$ -weight functions of these quasiparticle bands are given by $A_{\gamma,\pm}^f(\mathbf{k}) = A_{\gamma,+}^d(\mathbf{k}) = \frac{1}{2}[1 \pm \frac{\bar{\epsilon}_{f_\gamma} - \epsilon_{\mathbf{k}}}{\sqrt{(\bar{\epsilon}_{f_\gamma} - \epsilon_{\mathbf{k}})^2 + 4\bar{V}_\gamma^2}}]$, where $\bar{V}_\gamma = V_\gamma b$, and $\bar{\epsilon}_{f_\gamma} = \epsilon_f + \Delta_\gamma - \lambda_b$. In the zero temperature limit, $T = 0$, the upper bands are empty. Then the Fermi functions reduce to $f(E_{\gamma,+}(\mathbf{k})) = 0$, and $f(E_{\gamma,-}(\mathbf{k})) = \varphi_\gamma$ ($\sum_\gamma \varphi_\gamma = 4n$). Under the condition, $n = 2$ or $\varphi_\gamma = 1$, which holds as long as the chemical potential is within the hybridization gap, we obtain the following mean-field equations from Eqs. (2):

$$\bar{\epsilon}_{f_1} - \epsilon_f = \sum_{\Gamma=1,2} \frac{V_\Gamma^2}{2D} \ln \frac{\sqrt{(D - \bar{\epsilon}_{f_\Gamma})^2 + 4\bar{V}_\Gamma^2} + D - \bar{\epsilon}_{f_\Gamma}}{\sqrt{(D + \bar{\epsilon}_{f_\Gamma})^2 + 4\bar{V}_\Gamma^2} - D - \bar{\epsilon}_{f_\Gamma}}; \quad 2b^2 = \sum_{\Gamma=1,2} \left(\sqrt{(\bar{\epsilon}_{f_\Gamma} + D)^2 + 4\bar{V}_\Gamma^2} - (D \rightarrow -D) \right). \quad (3)$$

Here $\bar{\epsilon}_{f_2} = \bar{\epsilon}_{f_1} + \Delta_2$, $\bar{V}_2 = \bar{V}_1 + \delta\bar{V} = b(V_1 + \delta V)$, and $D = 6t$ is half the conduction band width. The density of states of the conduction band is assumed to be rectangular ($g(\epsilon) = 1/2D$; $-D < \epsilon < D$ and zero otherwise). By solving the set of equations numerically one can find the $\bar{\epsilon}_{f_1}$ and b values. In order to be in the Kondo limit and have an insulating state with small hybridization gap the parameters should fulfill the condition $\Delta_2 < \delta V < V_1$, $|\epsilon_f| < D$. In the absence of CEF effects, by choosing $\epsilon_f = -0.75t$, $V_1 = t$, $\delta V = 0$, $\Delta_2 = 0$ we found $\bar{\epsilon}_{f_1} = 0.05t$ and $b = 0.30$ from the mean-field solutions which will be used in Fig. 1. The dynamic magnetic susceptibility has the matrix form $\hat{\chi}(\mathbf{q}, \omega) = [I - \hat{J}_{\mathbf{q}} \hat{\chi}_0(\mathbf{q}, \omega)]^{-1} \hat{\chi}_0(\mathbf{q}, \omega)$, where the unit matrix I , the interaction $\hat{J}_{\mathbf{q}}$ and the noninteracting quasiparticle susceptibility $\hat{\chi}_0(\mathbf{q}, \omega)$ are 2×2 matrices in the CEF quartet index $\Gamma = 1, 2$. The exchange interaction $\hat{J}_{\mathbf{q}}$ between quasiparticles is assumed to be peaked at the antiferromagnetic (AFM) wave vector $\mathbf{Q} = (\pi, \pi, \pi)$, i.e., the L point because there the most pronounced magnetic response is found. In principle $\hat{J}_{\mathbf{q}}$ may be calculated to

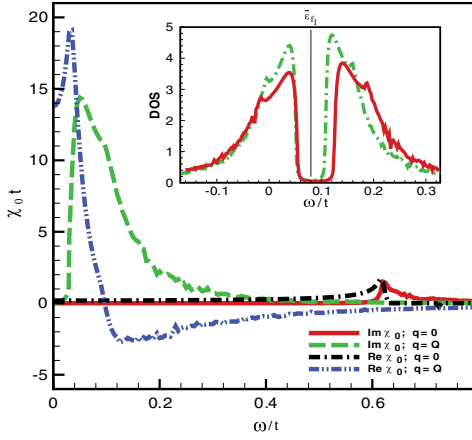


FIG. 1 (color online). Dynamical susceptibility in the [111] direction for $\mathbf{q} = \mathbf{0}$ (direct gap) and $\mathbf{q} = \mathbf{Q}$ (indirect gap) versus energy, for degenerate quasiparticle bands with $V_1 = t$ and $\delta V = 0$ ($\bar{V} = 0.30t$, $J_Q = 0$). Inset shows the density of states for two CEF-split quasiparticle bands ($\bar{\epsilon}_{f_1} = 0.08t$ and $b = 0.41$). The green curve corresponds to the band $V_1 = t$ and the red one to the band $V_2 = V_1 + 0.13t$.

order ($1/N^2$) [19,20] but this is strongly model dependent. We choose to parameterize $\hat{J}_{\mathbf{q}}$ in a simple way: The interaction is peaked at \mathbf{Q} or $Q = \sqrt{3}\pi$ and it has the Lorentzian form $J_{\mathbf{q}_{\Gamma\Gamma'}} = \frac{\Gamma_Q^2}{(\mathbf{q}-\mathbf{Q})^2 + \Gamma_Q^2} J_{\mathbf{Q}_{\Gamma\Gamma'}}$, where Γ_Q has the meaning of an inverse AFM correlation length. Each element of the irreducible susceptibility matrix is calculated from the quasiparticle states as [20]:

$$\chi_0^{\Gamma\Gamma'}(\mathbf{q}, \omega) = \sum_{\mathbf{k}, \pm} A_{\Gamma, \pm}^f(\mathbf{k} + \mathbf{q}) A_{\Gamma', \mp}^f(\mathbf{k}) \times \left[\frac{f(E_{\Gamma, \pm}(\mathbf{k} + \mathbf{q})) - f(E_{\Gamma', \mp}(\mathbf{k}))}{E_{\Gamma, \mp}(\mathbf{k}) - E_{\Gamma', \pm}(\mathbf{k} + \mathbf{q}) - \omega} \right]. \quad (4)$$

The nondiagonal elements of the interaction matrix corresponding to interactions of quasiparticles with different CEF symmetry are neglected, implying $J_{\mathbf{q}_{\Gamma\Gamma'}} = J_{\Gamma}(\mathbf{q})\delta_{\Gamma\Gamma'}$. Then the RPA susceptibility is simply a sum of two contributions $\chi^{\Gamma\Gamma}(\mathbf{q}, \omega)$ from the two sets of hybridized bands:

$$\chi(\mathbf{q}, \omega) = \sum_{\Gamma} [1 - J_{\Gamma}(\mathbf{q})\chi_0^{\Gamma\Gamma}(\mathbf{q}, \omega)]^{-1} \chi_0^{\Gamma\Gamma}(\mathbf{q}, \omega). \quad (5)$$

We now discuss the results of numerical calculations based on the previous analysis. In Fig. 1 we have plotted the real and imaginary part of $\chi_0^{\Gamma\Gamma}(\mathbf{q}, \omega)$ without CEF splitting ($\Delta_2 = \delta V = 0$) versus energy for wave vectors $\mathbf{q} = \mathbf{0}$ and $\mathbf{q} = \mathbf{Q}$. One notices that $\text{Im}\chi_0^{\Gamma\Gamma}(\mathbf{Q}, \omega)$ has a strong low-energy peak due to a small indirect gap while $\text{Im}\chi_0^{\Gamma\Gamma}(\mathbf{0}, \omega)$ has a small peak at much higher energy due to a large direct gap. The broad structure of the former is due to noninteracting single-particle excitations and the q and ω dependence is depicted in the inset of Fig. 4.

The density of states for noninteracting quasiparticles $\rho_{\gamma}(\omega) = \frac{1}{N_s} \sum_{\mathbf{k}, \pm} \delta(\omega - E_{\gamma, \pm}(\mathbf{k}))$ including the CEF splitting for the two sets of bands with $\Delta_2 = 0.01t$ and $\delta V = 0.13t$ is plotted in the inset of Fig. 1. The two hybridization gaps are different due to a finite δV . However, the latter is kept small enough to ensure that the chemical potential is within the gap.

When the AFM interaction $J_{\Gamma}(\mathbf{q})$ is turned on, the imaginary part becomes $\text{Im}\chi^{\Gamma\Gamma}(\mathbf{q}, \omega) = F(\alpha_{\Gamma}, \eta_{\Gamma})/J_{\Gamma}(\mathbf{q})$, $\alpha_{\Gamma} = J_{\Gamma}(\mathbf{q})\text{Im}\chi_0^{\Gamma\Gamma}(\mathbf{q}, \omega)$, $\eta_{\Gamma} = 1 - J_{\Gamma}(\mathbf{q})\text{Re}\chi_0^{\Gamma\Gamma}(\mathbf{q}, \omega)$, and $F(\alpha_{\Gamma}, \eta_{\Gamma}) = \alpha_{\Gamma}/(\eta_{\Gamma}^2 + \alpha_{\Gamma}^2)$. In that case the spectrum for $q = Q$ moves to lower energies and a narrow double-peak structure, i.e., the collective spin resonance excitations appear. Their energies ω_r are determined by the solution of $\eta_{\Gamma} = 0$. If they are lying within the indirect hybridization gap one has $\alpha_{\Gamma} \rightarrow 0$. Then the spectral function is a delta function $\pi\delta(\eta_{\Gamma})/J_{\Gamma}(\mathbf{q})$ at the resonance energy ω_r . The dispersion of the resonance, is determined by the real part of $\chi_0^{\Gamma\Gamma}(\mathbf{q}, \omega)$ presented in Fig. 2. The plot shows that for $q < Q$ the maximum of the spectral function follows a ridge which decreases in height and bends to higher energy. This turns into an upward dispersion of the resonance pole. Its endpoint in the BZ is limited by the extension of the ridge in $\text{Re}\chi_0$. The latter is fixed for the simple hybridization band model used here. A more realistic band model might give a larger extension than the one seen in Fig. 2.

Because of the CEF effect the f levels split into two (pseudo-) quartets ($\Delta_2 > 0$) which hybridize differently. For $\delta V > 0$ the resonance $\omega_r^{\Gamma=2}$ associated with the $\gamma = 2$ hybridized bands moves to higher energy and a second peak in addition to the one at $\omega_r^{\Gamma=1}$ appears in the spectral function. This is clearly seen in Fig. 3 where the CEF-split resonance peaks at $\mathbf{q} = \mathbf{Q}$ appear around the threshold energy of the noninteracting continuum states. In this figure we use subcritical values for the interaction constants. Therefore the resonance peaks are right above the continuum threshold and have a finite intrinsic line width.

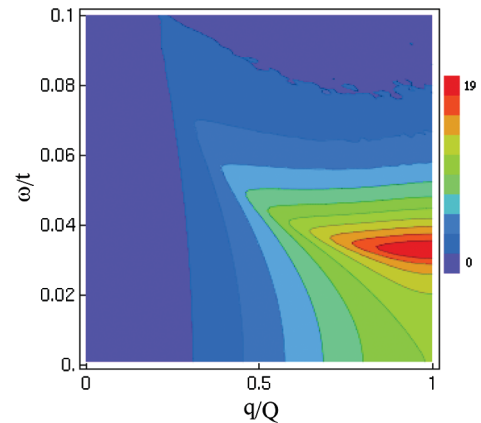


FIG. 2 (color). Contour plot of the real part of noninteracting dynamical susceptibility for degenerate bands with $V_1 = t$ and $\delta V = 0$ ($\bar{V}_1 = 0.30t$, $J_Q = 0$) in the [111] direction.

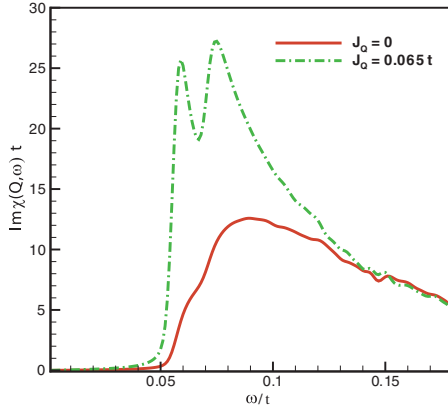


FIG. 3 (color online). The imaginary part of the susceptibility for the noninteracting ($J_Q = 0$) and interacting case ($J_{Q_1} = J_{Q_2} = 0.065t$) for $V_1 = t$, $\mathbf{q} = \mathbf{Q}$ and $\delta V = 0.13t$. The J_{Q_i} are slightly subcritical leading to a finite intrinsic resonance line width.

If the interaction constants are slightly increased the resonances move below the continuum and turn into true spin exciton poles without intrinsic line widths (within RPA). Their dispersion is shown in the main panel of Fig. 4. Away from the L point ($Q = \sqrt{3}\pi$) they disperse

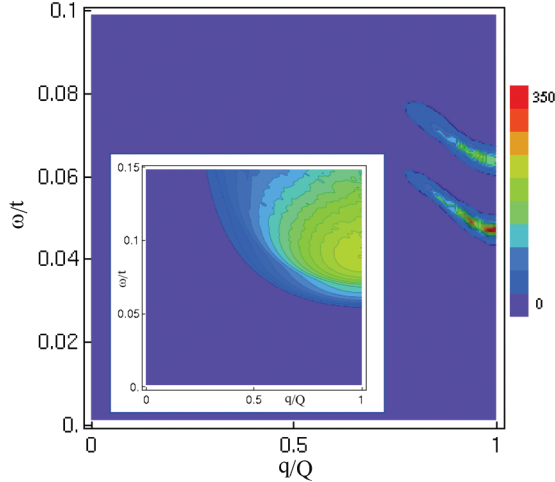


FIG. 4 (color). Contour plot of imaginary part of RPA dynamical susceptibility with Lorentzian interaction $J_\Gamma(q)$ for CEF-split quasiparticle bands, $\bar{\epsilon}_{f_1} = 0.08t$ and $b = 0.41$. Here $V_1 = t$ and $V_2 = V_1 + 0.13t$ ($J_{Q_1} = 0.125t$, $J_{Q_2} = 0.143t$ and $\Gamma_Q = 2$ which satisfy the resonance condition in RPA formula: $J_\Gamma(\mathbf{Q}) = 1/\text{Re}[\chi_0^{\Gamma\Gamma}(\mathbf{Q}, \omega_r)]$), in the $[111]$ direction. The peaks at the zone boundary ($\mathbf{q} = \mathbf{Q}$) appear at $\omega_1 = 0.047t$ and $\omega_2 = 0.063t$. By choosing $t = 0.32$ eV ($D = 1.92$ eV) then $\omega_1 = 15$ meV and $\omega_2 = 20$ meV which are comparable with experimental results. The inset shows the contour plot of imaginary part of dynamical susceptibility of noninteracting degenerate bands for comparison ($V_1 = t$, $\delta V = 0.13t$, $\bar{V}_1 = 0.41t$, and $J_Q = 0$) in the $[111]$ direction. The color scale of the inset is the same as in Fig. 2.

upwards and merge into the continuum. We identify these spin resonance modes with the observed experimental peaks at 15 and 20 meV [7,9] and we have chosen parameters such that their energy splitting and dispersion are reproduced. Our numerical calculations show that the best fit to experiments is obtained for $\delta V = 0.13t$, where $\bar{\epsilon}_{f_1} = 0.08t$ and $b = 0.41$. These spin exciton peaks separate with increasing CEF splitting Δ_2 and hybridization energy difference δV . Therefore the influence of the latter is strong since it directly affects the hybridization gap and hence the noninteracting susceptibility and resonance condition. We note that an increase in J_Q (or a decrease of the hybridization gap) will lead to a decrease of the spin exciton mode frequencies at \mathbf{Q} . For $J_{Q_1} = 0.179t$ the lowest mode would become soft. This softening signifies the instability of the paramagnetic state and the onset of AFM order in a Kondo semiconductor. This is not observed in YbB_{12} at ambient pressure. We suggest that an investigation of the pressure dependence of spin exciton mode frequencies at \mathbf{Q} would give important clues how close YbB_{12} is to AFM order. Finally, we mention that our present model does not include the broad excitations at 38 meV. This might be due to a continuum of additional band states which do not take place in the resonance formation [13]. Their inclusion would require a multiorbital conduction band model.

We thank P.A. Alekseev and I. Eremin for helpful discussions.

-
- [1] G. Aeppli and Z. Fisk, *Comments Condens. Matter Phys.* **16**, No. 3, 155 (1992).
 - [2] M.F. Hundley *et al.*, *Phys. Rev. B* **42**, 6842 (1990).
 - [3] M. Kasaya *et al.*, *J. Magn. Magn. Mater.* **31–34**, 437 (1983).
 - [4] F. Iga, N. Shimizu, and T. Takabatake, *J. Magn. Magn. Mater.* **177–181**, 337 (1998).
 - [5] P.S. Riseborough, *Adv. Phys.* **49**, 257 (2000).
 - [6] T. Susaki *et al.*, *Phys. Rev. Lett.* **82**, 992 (1999).
 - [7] K.S. Nemkovski *et al.*, *Phys. Rev. Lett.* **99**, 137204 (2007).
 - [8] H. Okamura *et al.*, *J. Phys. Soc. Jpn.* **74**, 1954 (2005).
 - [9] J.-M. Mignot *et al.*, *Phys. Rev. Lett.* **94**, 247204 (2005).
 - [10] E. V. Nefedova *et al.*, *Phys. Rev. B* **60**, 13 507 (1999).
 - [11] A. Bouvet *et al.*, *J. Phys. Condens. Matter* **10**, 5667 (1998).
 - [12] I. Eremin *et al.*, *Phys. Rev. Lett.* **101**, 187001 (2008).
 - [13] J.-M. Mignot *et al.*, *Physica (Amsterdam)* **383B**, 16 (2006).
 - [14] Alekseev *et al.*, *J. Phys. Condens. Matter* **16**, 2631 (2004).
 - [15] P.S. Riseborough, *J. Magn. Magn. Mater.* **226–230**, 127 (2001).
 - [16] S.H. Liu, *Phys. Rev. B* **63**, 115108 (2001).
 - [17] P. Coleman, *Phys. Rev. B* **29**, 3035 (1984).
 - [18] P.A. Alekseev (private communication).
 - [19] S. Doniach, *Phys. Rev. B* **35**, 1814 (1987).
 - [20] P.S. Riseborough, *Phys. Rev. B* **45**, 13 984 (1992).